

Published in final edited form as:

Structure. 2013 September 3; 21(9): 1612–1623. doi:10.1016/j.str.2013.07.003.

The differential regulation of p38 α by the neuronal KIM-PTPs, a detailed molecular study

Dana May Francis^{a,§}, Ganesan Senthil Kumar^{a,§}, Dorothy Koveal^b, Antoni Tortajada^b, Rebecca Page^b, and Wolfgang Peti^{a,c,*}

^aDepartment of Molecular Pharmacology, Physiology and Biotechnology, Brown University, Providence RI, 02912, USA

^bDepartment of Molecular Biology, Cell Biology and Biochemistry, Brown University, Providence RI, 02912, USA

^cDepartment of Chemistry, Brown University, Providence RI, 02912, USA

Summary

The MAP kinase p38 is essential for neuronal signaling. To better understand the molecular regulation of p38 we used atomistic and molecular techniques to determine the structural basis of p38 regulation by the two neuronal tyrosine phosphatases, PTPSL/PTPBR7 (PTPRR) and STEP (PTPN5). We show that, despite the fact that PTPSL and STEP belong to the same family of regulatory proteins, they interact with p38 differently and their distinct molecular interactions explain their different catalytic activities. While the interaction of PTPSL with p38 is similar to that of the previously described p38:HePTP (PTPN7) complex, STEP binds and regulates p38 in an unexpected and new manner. Using NMR and small angle X-ray scattering data we generated a model of the p38:STEP complex and define molecular differences between its resting- and active-states. Together, these results provide fundamentally new insights into molecular regulation of p38 by key regulatory proteins.

INTRODUCTION

The mitogen-activation protein kinases (MAPKs), p38, ERK and JNK, are central to evolutionarily conserved signaling pathways that are present in all eukaryotic cells. Each MAPK cascade is activated in response to a diverse array of extracellular signals and culminates in the dual-phosphorylation of a threonine and a tyrosine residue in the MAPK activation loop (Derijard et al., 1995). Dually phosphorylated MAPKs then phosphorylate both cytosolic and nuclear targets, with the localization and duration of MAPK activity determining the cellular response to the initial extracellular signal. MAPK signal duration is finely controlled by multiple phosphatases, including three kinase-interaction motif-protein tyrosine phosphatases (KIM-PTPs): PTPSL/PTPBR7 (PTPRR), STEP (PTPN5), HePTP

© 2013 Elsevier Inc. All rights reserved.

*Corresponding Author: Wolfgang_Peti@brown.edu, phone: (401) 863-6084, fax: (401) 863-6087.

§authors contributed equally

SUPPLEMENTAL INFORMATION

Supplemental Information includes figures and Supplemental Experimental Procedures and can be found with this article online at <http://>

Publisher's Disclaimer: This is a PDF file of an unedited manuscript that has been accepted for publication. As a service to our customers we are providing this early version of the manuscript. The manuscript will undergo copyediting, typesetting, and review of the resulting proof before it is published in its final citable form. Please note that during the production process errors may be discovered which could affect the content, and all legal disclaimers that apply to the journal pertain.

(PTPN7, LC-PTP) (Hendriks et al., 1995; Lombroso et al., 1991; Zanke et al., 1992). KIM-PTPs control MAPK signaling by two mechanisms: 1) the KIM-PTP binds to an unphosphorylated MAPK to sequester it in the cytosol (known as the resting-state complex); or 2) the KIM-PTP dephosphorylates and inactivates a phosphorylated MAPK (known as the active-state complex) (Tarrega et al., 2002; Xu et al., 2009).

Increasing evidence suggests a crucial role for MAPK signaling in the central nervous system (CNS) and aberrant phosphorylation within the CNS is associated with a multitude of neurological disorders, including Alzheimer's and Parkinson's disease (Kim and Choi, 2010). Correspondingly, an additional layer of MAPK regulation is present within neurons. Two KIM-PTPs, PTPSL and STEP, are expressed within discrete regions of the CNS. PTPSL expression is highest in the cerebellum, while STEP is expressed in the hippocampus, striatum, amygdala and cortex (Chirivi et al., 2004; Lombroso et al., 1993; Van Den Maagdenberg et al., 1999).

PTPSL, STEP and the other KIM-PTP, HePTP, have a 17-residue kinase-interaction motif (KIM or D-motif) that is essential for their interaction with ERK2 and p38 (Blanco-Aparicio et al., 1999; Saxena et al., 1999). The KIM binds to a conserved binding site that is formed by the hydrophobic docking groove and an acidic patch named the common docking (CD) site (together known as the KIM-binding site or D-motif recruitment site) (Tarrega et al., 2002; Zhou et al., 2006). The KIM sequence is well conserved across the KIM-PTP family. All three KIMs contain basic residues, proposed to engage the CD site, upstream of a hydrophobic motif (L-X-L-X- , where X is a methionine in STEP and PTPSL and a valine in HePTP; Figure 1A). Previously, we used nuclear magnetic resonance (NMR) spectroscopy and isothermal titration calorimetry (ITC) to define the interface of HePTP_{KIM} binding to p38 . We determined that the hydrophobic motif occupies three hydrophobic pockets within the p38 hydrophobic docking groove, while its basic residues interact with the acidic patch (Francis et al., 2011a).

C-terminal to the KIM is a region known as the kinase-specificity sequence (KIS) which is followed by a globular PTP catalytic domain (CAT) (Eswaran et al., 2006; Munoz et al., 2003; Mustelin et al., 2005). While the CAT is essential for dephosphorylation of the MAPK by the KIM-PTP, the importance of the KIS remains ambiguous, especially as the KIS sequence is divergent among the KIM-PTP family members. We previously showed that the HePTP_{KIS} is highly flexible and contributes significantly to the interaction between HePTP and p38 , while HePTP_{CAT} does not interact with unphosphorylated p38 . This was corroborated by small-angle x-ray scattering (SAXS) experiments that showed that the p38 :HePTP resting-state complex is elongated in solution (Francis et al., 2011a). Whether the extensive KIS interaction, limited CAT interaction and extended resting-state conformation observed in p38 :HePTP are common features of all p38 :KIM-PTP resting-state complexes is currently unknown.

Similar studies with a different MAPK, ERK2, revealed that the ERK2:HePTP resting-state complex shares several of these features. As with p38 , HePTP_{CAT} does not interact with ERK2 in the resting-state, and the ERK2:HePTP resting-state complex is extended in solution (Piserchio et al., 2012). However, phosphorylation of ERK2 leads to a domain rearrangement in which HePTP_{CAT} rotates by nearly 180°, the ERK2:HePTP complex compacts and the HePTP catalytic site residue moves by ~65 Å to allow for dephosphorylation of ERK2 (Francis et al., 2011b). The flexibility of the HePTP_{KIS} and the absence of an interaction between ERK2 and HePTP_{CAT} are critical to facilitate this large rearrangement.

Here, we combined NMR, SAXS, ITC experiments and HADDOCK to delineate the interaction of p38 with STEP and PTPSL. In combination with experiments conducted with HePTP, these studies serve as the first atomic-level characterization of MAPK regulation by an entire family of regulators – the KIM-PTP family. Our results reveal key differences between the interactions of p38 with each KIM-PTP. We show that the interaction of p38 with PTPSL is closely related to the interaction of HePTP, while the interaction of p38 with STEP is quite different and includes an unexpected contribution from STEP_{CAT}.

RESULTS

KIM binding to p38 α is conserved within the KIM-PTP family

We used NMR spectroscopy to define the p38 binding interface of the STEP_{KIM} and PTPSL_{KIM} peptides (constructs used in this study are illustrated in Figure 1B). Each peptide was individually titrated into [²H,¹⁵N]-p38 until binding was saturated (1:1, 1:3, 1:5, 1:8 molar ratio of p38 :peptide) and two-dimensional (2D) [¹H,¹⁵N] TROSY spectra were recorded (Figure 1C, D; Supplemental Figure S1A). The fully saturated 2D [¹H,¹⁵N] TROSY spectra of p38 :PTPSL_{KIM} and p38 :STEP_{KIM} (100 μ M [²H,¹⁵N]-p38 :800 μ M peptide) are highly similar (Figure 1E; Supplemental Figure S1B). All peak shifts are in fast exchange and can be readily followed with the exception of 3 peaks that map to the MAPK-specific insert (L262-Q264) and are broadened beyond detection independent of ligand (Supplemental Figure S1A). As expected, both peptides caused significant chemical shift perturbations (CSPs) for residues located in the KIM-binding site, including helix D, helix E, the D–E loop, the 7–8 turn, loop 4 and the CD site (Figure 2). Thus, like HePTP_{KIM}, PTPSL_{KIM} and STEP_{KIM} engage all three hydrophobic pockets and interact with the acidic patch demonstrating that the mode of KIM binding to p38 is conserved within the KIM-PTP family.

However, there are small differences between the CSPs induced by STEP_{KIM} and PTPSL_{KIM}. L164 in 8 exhibits the largest CSP difference between the 2D [¹H,¹⁵N] TROSY spectra of p38 :PTPSL_{KIM} and p38 :STEP_{KIM} (Figure 1E; Supplemental Figure S1B). The N-terminal residues of the KIM (Ile in PTPSL_{KIM}; Met in STEP_{KIM}) are the only residues not identical between the two peptides; therefore, any differences between the two spectra are a result of the differential interaction of this residue with p38. Based on the structure of ERK2:HePTP_{KIM}, this residue is immediately adjacent to the 7–8 turn further supporting our NMR results (Zhou et al., 2006).

Although the KIM binding mode is conserved among the KIM-PTPs, the HePTP_{KIM} sequence is only ~75% conserved when compared with PTPSL_{KIM} and STEP_{KIM} (Figure 1A). This leads to changes in the chemical environment for residues within the p38 KIM-binding site, which are readily observed in the 2D [¹H,¹⁵N] TROSY spectra (Supplemental Figure S1C). PTPSL_{KIM} and STEP_{KIM} perturb 9 more peaks than HePTP_{KIM} (Francis et al., 2011a). Compared to HePTP_{KIM}, PTPSL_{KIM} and STEP_{KIM} interact differentially with several residues within the hydrophobic binding groove and loop 4, including N82, A111, L113, C119, L122, D124, D125, V127, L130, S154, E160, C162 and L164 (Figure 1E). These NMR CSP experiments correspond well with ITC measurements that showed PTPSL_{KIM} and STEP_{KIM} bind p38 ~2-times tighter than HePTP_{KIM} (Table 1; Supplemental Figure S2).

An NMR view of the interaction between PTPSL and p38 α

We expanded the NMR experiments to define the binding interface of PTPSL with p38. In this experiment, [²H,¹⁵N]-p38 was incubated with unlabeled PTPSL, the 78 kDa

p38 :PTPSL complex was purified by size exclusion chromatography (SEC) and a 2D [^1H , ^{15}N] TROSY spectrum was immediately recorded (Supplemental Figure S3C).

Direct comparison of the 2D [^1H , ^{15}N] TROSY spectra of free and PTPSL-bound p38 reveals CSPs of 41 peaks, 36 in fast exchange and 5 peaks with line-widths broadened beyond detection (N115, Q120, F129, L130, S154; Figure 2). Like PTPSL_{KIM}, PTPSL perturbed residues clustered within the hydrophobic binding groove and the acidic patch of p38 (Figure 2). Two peaks, N115 (line-widths broadened beyond detection) and V127, are perturbed by full-length PTPSL but not by PTPSL_{KIM} with additional peaks experiencing larger CSPs (G110, D112, I116, K118, Q120, Q310) (Figure 2). Correspondingly, full-length PTPSL binds ~7-times tighter to p38 than PTPSL_{KIM} (Table 1; Supplemental Figure S2).

The majority of the additional CSPs map to a region of p38 that interacts with HePTP_{KIS} (Francis et al., 2011a). While the PTPSL_{KIS} and HePTP_{KIS} sequences are only ~50% conserved, this region of p38 is thus also likely interacting with PTPSL_{KIS}. To determine if a peptide composed of the PTPSL_{KIM} and PTPSL_{KIS} sequences (i.e. PTPSL_{KIMKIS}) can recapitulate the binding of full-length PTPSL to p38, we titrated the PTPSL_{KIMKIS} into [^2H , ^{15}N]-p38 and a series of 2D [^1H , ^{15}N] TROSY spectra were recorded (Supplemental Figure S3B). Titration of a 3-fold molar excess of the PTPSL_{KIMKIS} peptide (100 μM [^2H , ^{15}N]-p38 :300 μM PTPSL_{KIMKIS}) resulted in a nearly identical 2D [^1H , ^{15}N] TROSY spectrum as that of p38 :PTPSL (Figure 2, Supplemental Figure S3H). Differences include residues N115 and S154, which are broadened beyond detection by full-length PTPSL but are either not perturbed (N115) or undergo a large CSP (S154) with PTPSL_{KIMKIS}, respectively (Supplemental Figure S3H). Furthermore, a direct comparison of the 2D [^1H , ^{15}N] TROSY spectra of p38 :PTPSL_{KIM} with p38 :PTPSL_{KIMKIS} shows larger CSPs for four residues (M109, K118, E160, L164), and three peaks (Q120, F129, L130) are broadened beyond detection by PTPSL_{KIMKIS} but not by PTPSL_{KIM} (Supplemental Figure S3H). Consistent with these results, the PTPSL_{KIMKIS} binds p38 ~2-times tighter than PTPSL_{KIM} (Table 1; Supplemental Figure S2).

The p38 α :PTPSL resting-state complex is extended in solution

The interactions of PTPSL_{KIM}, PTPSL_{KIMKIS} and PTPSL with p38 are highly similar. PTPSL perturbed few residues outside of the KIM-binding site confirming that the KIM is the essential anchor for the interaction of PTPSL with p38. Indeed, we used NMR spectroscopy to probe the interaction of p38 with PTPSL_{CAT}, a construct lacking residues 332–360, which includes the KIM; no interactions between p38 and isolated PTPSL_{CAT} were detected (Supplemental Figure S4A, C). This is consistent with previous results from NMR experiments which showed that the isolated HePTP_{CAT} did not interact with either p38 or ERK2 (Francis et al., 2011a; Piserchio et al., 2012).

Consequently, we used SAXS to determine the size and shape of the p38 :PTPSL resting-state complex. The p38 :PTPSL complex was purified by SEC, and SAXS data was recorded at Beamline X9A at the National Synchrotron Light Source (Brookhaven National Laboratories). Using the Guinier approximation of five independent SAXS samples, a radius of gyration (R_g) of 33.1 ± 0.5 Å was calculated for the p38 :PTPSL complex (Table 2; Figure 3A). A maximum particle dimension (D_{max}) of 105 Å was determined by analysis of the $P(r)$ function (Table 2; Figure 3D, E). These values for R_g and D_{max} are highly similar to those determined for the p38 :HePTP and ERK2:HePTP resting-state complexes and demonstrate that, under resting conditions, p38 and PTPSL adopt an extended conformation, with a rather limited interaction surface, consistent with the NMR CSP experiments.

The p38 α :STEP resting-state complex is compact

Equivalent SAXS measurements were performed for the p38 α :STEP resting-state complex. The Guinier approximation of four independent SAXS samples was used to calculate an R_g of 29.9 ± 0.3 Å, showing that the R_g of the p38 α :STEP resting-state complex is ~ 3.0 Å smaller than that of the p38 α :PTPSL and p38 α :HePTP resting-state complexes (Table 2; Figure 3B). To analyze this difference in more detail, we determined the molecular envelope of the p38 α :STEP resting-state complex (Table 2; Figure 3D, F). A D_{max} of 95 Å was determined by analysis of the $P(r)$ function, which is ~ 10 – 15 Å shorter than the p38 α :PTPSL and p38 α :HePTP complexes (Table 2; Figure 3D). Thus, the p38 α :STEP resting-state complex is more compact than both the p38 α :KIM-PTP and the ERK2:HePTP resting-state complexes. Therefore, unlike PTPSL and HePTP, which have limited interaction surfaces with p38 α , this result suggested that STEP may interact more extensively with p38 α .

STEP has interactions with p38 α outside of the KIM binding pocket

To test this hypothesis, we performed NMR CSP experiments with full-length STEP and [$^2\text{H}, ^{15}\text{N}$]-p38 α . Here, [$^2\text{H}, ^{15}\text{N}$]-p38 α was incubated with unlabeled STEP, the 78 kDa p38 α :STEP complex purified by SEC, and a 2D [$^1\text{H}, ^{15}\text{N}$] TROSY spectrum recorded (Supplemental Figure S3F). Direct comparison of the 2D [$^1\text{H}, ^{15}\text{N}$] TROSY spectra of free and STEP-bound p38 α reveals CSPs of 58 peaks, 40 in fast exchange and 18 with peak line-widths that are broadened beyond detection (Figure 2). As expected, like STEP_{KIM}, STEP perturbs residues in the p38 α KIM-binding site (Figure 2). Surprisingly, STEP perturbed significantly more residues in p38 α than STEP_{KIM} and caused several additional peaks to broaden beyond detection, decreasing the total number of peaks in the 2D [$^1\text{H}, ^{15}\text{N}$] TROSY spectrum of STEP-bound p38 α (Figure 2). Direct comparison of the 2D [$^1\text{H}, ^{15}\text{N}$] TROSY spectra of p38 α :STEP_{KIM} and p38 α :STEP reveals three additional residues (V30, M109, L164) with CSPs and 18 additional peaks (D125, V127, Y132, I141, S154, D177, M179, V183, A190, Q202, R220, L222, L247, K248, S254, R256, H312, E328) that are broadened beyond detection by full-length STEP (Supplemental Figure S3I). Correspondingly, full-length STEP binds ~ 6 -times tighter to p38 α than STEP_{KIM} (Table 1; Supplemental Figure S2). Mapping the additional perturbations reveals a previously undetected p38 α interaction surface (herein referred to as the PTP-site), which connects the p38 α activation loop to the MAPK-specific insert.

To corroborate our findings, we used a divide and conquer approach. To determine if the STEP_{KIS} accounts for this additional interaction, a peptide composed of the STEP_{KIMKIS} sequence was titrated into [$^2\text{H}, ^{15}\text{N}$]-p38 α , and a series of 2D [$^1\text{H}, ^{15}\text{N}$] TROSY spectra were recorded (Supplemental Figure S3E). Interestingly, the p38 α :STEP_{KIMKIS} spectrum (100 μM [$^2\text{H}, ^{15}\text{N}$]-p38 α :800 μM STEP_{KIMKIS}) is similar to that of p38 α :STEP_{KIM} at the same molar ratio (Figure 2; Supplemental Figure S3I). Direct comparison of the 2D [$^1\text{H}, ^{15}\text{N}$] TROSY spectra of p38 α :STEP_{KIM} and p38 α :STEP_{KIMKIS} reveals differences in seven residues: V30, M109 and E160 show CSPs, while G85, D125, V127 and S154 are broadened beyond detection (Supplemental Figure S3I). Using ITC we determined that STEP_{KIMKIS} binds ~ 2.5 -times tighter than STEP_{KIM} but 2-times weaker than full-length STEP (Table 1; Supplemental Figure S2). Importantly, the STEP_{KIMKIS} did not affect residues within the new PTP-site (Figure 2). This suggests that the additional changes in the NMR spectrum must be the result of an interaction between the STEP catalytic domain (STEP_{CAT}) and p38 α .

p38 α :PSChimera complex

To confirm that STEP_{CAT} interacts directly with p38 α , we generated a chimeric protein in which PTPSL_{KIMKIS} was fused with STEP_{CAT} (herein referred to as the PSChimera; Figure

1B). The PSChimera was expressed, purified and incubated with $[^2\text{H}, ^{15}\text{N}]$ -p38. The p38 :PSChimera complex was then purified by SEC and a 2D $[^1\text{H}, ^{15}\text{N}]$ TROSY spectrum of the complex was recorded (Supplemental Figure S3G).

Within and around the p38 KIM binding site, the PSChimera affected the p38 2D $[^1\text{H}, ^{15}\text{N}]$ TROSY spectrum in a PTPSL-like manner (Figure 2). Notably, additional changes in the p38 2D $[^1\text{H}, ^{15}\text{N}]$ TROSY spectrum, which correspond to peaks that define the newly identified PTP-site, were also identified (Figure 2). Thus, the PSChimera, which has a PTPSL_{KIMKIS} and a STEP_{CAT} domain, interacts in a PTPSL-like manner with its KIMKIS and a STEP-like manner at the PTP-site. Minor differences between the interaction of the PSChimera and STEP with p38 at the PTP-site include Q202 and K248 that are not broadened beyond detection with PSChimera (K248 does experience a small CSP). Similar to STEP, 17 peaks in the PTP-site broaden beyond detection with PSChimera, demonstrating that the STEP_{CAT} interaction with p38 is independent of the KIMKIS sequence. Furthermore, NMR interaction studies showed that titration of unlabeled, isolated STEP_{CAT} (lacking residues 214–243 including the KIM) with $[^2\text{H}, ^{15}\text{N}]$ -p38 results in non-specific interactions throughout the p38 surface, – further reinforcing the critical importance of KIM anchoring for p38 regulation (Supplemental Figure S4B, C). The chimeric protein has a slightly higher binding affinity than PTPSL or STEP for p38 (Table 1). This binding affinity is the product of the PTPSL_{KIM}, which binds the tightest of the three KIM-PTP_{KIM} peptides, coupled with the additional binding strength afforded by the STEP_{CAT} interaction.

Defining the p38 α binding site on STEP

To define the p38 binding interface on STEP, we performed reverse NMR experiments with $[^2\text{H}, ^{15}\text{N}]$ -STEP and unlabeled p38. We previously published the sequence-specific backbone assignments of STEP_{CAT} (Francis et al., 2013). The 2D $[^1\text{H}, ^{15}\text{N}]$ TROSY spectrum of STEP contains 30 additional peaks when compared to that of STEP_{CAT}, in agreement with the 31 additional N-terminal residues in STEP (Supplemental Figure S4D). All new peaks cluster around ~8.0 ppm, a chemical shift range typical for unstructured residues, suggesting that the KIM and KIS regions of STEP are unstructured in the unbound state, identical to what we have seen for HePTP (Supplemental Figure S4D) (Francis et al., 2011a). Lastly, the vast majority of peaks in the STEP 2D $[^1\text{H}, ^{15}\text{N}]$ TROSY spectrum overlap perfectly with peaks in the STEP_{CAT} 2D $[^1\text{H}, ^{15}\text{N}]$ TROSY spectrum, showing that the flexible N-terminal residues in STEP do not interact with STEP_{CAT}. This allowed for the transfer of the STEP_{CAT} sequence-specific backbone assignment to STEP.

Peaks corresponding to residues 244–253, the majority of helix 0, have very different chemical shifts between STEP and STEP_{CAT}, indicating that the presence of the flexible N-terminus (residues 214–243) alters the chemical environment of residues 244–253. This is consistent to what was observed for HePTP, in which helix 0 (residues 44–56) was also perturbed by the presence of the N-terminus, residues 15–43 (Francis et al., 2011a). Previously, it was hypothesized that helix 0 must change conformation in order for the regulatory Ser/Thr residue at the N-terminus of the helix to be phosphorylated (Mustelin et al., 2005; Szedlacsek et al., 2001). These NMR studies show that this hypothesis is correct and the pliability of helix 0 is conserved within the KIM-PTP family.

To test the effects of p38 binding on STEP, the complex between $[^2\text{H}, ^{15}\text{N}]$ -STEP and unlabeled p38 was purified by SEC, and a 2D $[^1\text{H}, ^{15}\text{N}]$ TROSY spectrum of the 78 kDa complex was immediately collected (Supplemental Figure S4E). Direct comparison of the 2D $[^1\text{H}, ^{15}\text{N}]$ TROSY spectra of free and p38-bound STEP reveals changes in 54 peaks, 22 of which are in fast exchange and 32 with peak line-widths broadened beyond detection (Figure 4A; Supplemental Figure S4E). Included in this total are 21 of the new peaks that

clustered around 8.0 ppm in the free STEP spectrum that are broadened beyond detection or overlap with other peaks in the in the 2D [¹H, ¹⁵N] TROSY spectrum of the p38 :STEP complex. This indicates, as expected, a strong involvement of the STEP_{KIM} in p38 binding. Additional new peaks unperturbed by p38 binding originate from STEP_{KIS} residues that do not contribute to p38 binding. 33 perturbed peaks are in STEP_{CAT}, including residues in helix -1 (A263, E268, K269), helix -2 (F274, L276, E277, A278, E279, F280, F281, E282), the 4–7 loop (N376, I377, E378, E379, M380), helix 4 (R478, T479, F482) and helix -6 (T517, C518, Q520, H525) (Figure 4A). Other STEP_{CAT} residues that are affected include: L254, A257, M285, N286, D294, T306, I307, G350, V353 and the catalytically important Q516 (Figure 4A).

3D model of the p38 α :STEP complex

We used the NMR data, which describe the interaction interface of STEP on p38 and vice versa, together with surface accessibility data, to restrain the docking of STEP and p38 using HADDOCK (the crystal structures of apo-p38 (1P38) and STEP_{CAT} (2BIJ) (de Vries et al., 2007; Dominguez et al., 2003; Eswaran et al., 2006; Wang et al., 1997) were used as starting structures). While the STEP_{CAT} structure does not include STEP_{KIMKIS} residues (214–257), we have established – using the PSChimera – that the STEP_{CAT} interaction occurred independent of a specific KIMKIS sequence. Consequently, only p38 residues affected by STEP_{CAT} in both STEP and the PSChimera were used as input for the HADDOCK calculations. The lowest energy cluster produced by HADDOCK contained 76 structures with an RMSD of 0.8 Å. The four lowest energy structures from this cluster are shown in Figure 4B. In all HADDOCK models, STEP helix -2 binds to p38 between the activation loop and the MAPK-specific insert. The interface between the two proteins buries $2125 \pm 116 \text{ \AA}^2$ of surface area. To experimentally test the validity of the model, we compared the calculated (determined using Hydropro (Ortega et al., 2011)) R_g of the lowest energy p38 :STEP HADDOCK model ($R_g = 29.2 \text{ \AA}$) with the experimentally determined R_g ($R_g = 29.9 \text{ \AA}$). The excellent consistency of the R_g 's is further supported by the excellent fit of the lowest energy p38 :STEP HADDOCK model into the molecular envelope determined for the p38 :STEP resting-state complex (NSD = 1.7; Figure 4C). Additionally, modeling the KIM peptide into the KIM-binding site of p38 (based on the ERK2:HePTP_{KIM} crystal structure (Zhou et al., 2006)) results, as expected, a further improved model of the p38 :STEP resting-state complex ($R_g = 30.1 \text{ \AA}$; $D_{\text{max}} = 92 \text{ \AA}$). This model, which is comprised of every component of the complex but the STEP_{KIS}, superimposes even better with the p38 :STEP molecular envelope (NSD = 1.5; Figure 4C) (Kozin and Svergun, 2001).

To further verify the model of the p38 :STEP resting-state complex, we generated a number of STEP mutants that are predicted to lead to changes in binding affinity, as the mutated residues are directly involved in the p38 :STEP interaction. Indeed, mutations of residues in helix -2, and to a lesser extent residues C-terminal to helix -2, showed a reduction of the binding affinity, clearly showing that helix -2 is important for the interaction of STEP with p38 and further confirming the HADDOCK model (Table 1).

The p38 α :STEP active-state complex

We have shown that STEP_{CAT}, when tethered via the KIM, interacts with p38 and perturbs residues in the p38 activation loop. However, this does not imply that STEP is poised and ready to efficiently dephosphorylate p38. In fact in the HADDOCK p38 :STEP resting-state complex model, the STEP active site cysteine is $\sim 35 \text{ \AA}$ away from the p38 phosphorylation loop tyrosine. Therefore, a domain arrangement must occur between the resting- and active-states of the p38 :STEP complex to properly position STEP_{CAT} for dephosphorylation of p38.

To verify that a domain rearrangement occurs between the active- and resting-states of the p38 :STEP complex, we used SAXS to determine the size and shape of the p38 :STEP active-state complex (Akella et al., 2010; Nielsen and Schwalbe, 2011). p38 was dually phosphorylated *in vitro* using a constitutively active mutant of MKK6. Phosphorylated p38 was incubated with a substrate trapping mutant of STEP (C472S/T306D), the complex purified by SEC, and SAXS data recorded (Figure 5A). Using the Guinier approximation of six independent SAXS samples, an R_g of $28.5 \pm 0.3 \text{ \AA}$ was calculated for the p38 :STEP active-state complex (Table 2; Figure 5A). This R_g is 1.5 \AA smaller than the R_g of the resting-state complex. More strikingly, the D_{max} of the active-state complex, 80 \AA , is 15 \AA shorter than the resting-state complex (Table 2; Figure 5C, D). These data show that the p38 :STEP active-state complex is more compact than the resting-state complex and support that a domain rearrangement occurs between the resting- and active-states of the p38 :STEP complex. Thus, although STEP_{CAT} interacts with p38 in the resting-state, it is not properly positioned for dephosphorylation of p38 .

DISCUSSION

Our current understanding of MAPK regulation by their regulatory proteins at the molecular level is extremely limited, as these essential signaling complexes have proven exceedingly difficult to investigate using traditional structural approaches. Years of efforts to crystallize MAPK:KIM-PTP complexes have not been successful, and their large molecular weights, ~80 kDa, make NMR analysis onerous. To circumvent these problems, we examined the binding of each domain of STEP and PTPSL to p38 using NMR CSP and ITC experiments and then determined the overall molecular shape of the complexes using SAXS. Using this approach, we show that, despite having similar KIM-peptide interactions and overall binding affinities with p38 , the p38 :PTPSL and p38 :STEP resting-state complexes are surprisingly different due to an additional interaction of the STEP catalytic domain with p38 . These studies, in combination with complementary studies previously performed between p38 and HePTP, provide the first detailed investigation of MAPK regulation by an entire family of regulators (Francis et al., 2011a).

Using NMR experiments, we show that the mode of KIM binding to p38 is conserved among the KIM-PTP family. Uniformly, PTPSL_{KIM}, STEP_{KIM} and HePTP_{KIM} engaged residues within the three hydrophobic pockets and perturbed residues at the CD site. In contrast, crystal structures of p38 bound to KIM peptides of the activating kinases, MKK3b and MKK6, reveal a different mode of binding in which only hydrophobic pockets _A and _B are engaged and an extensive electrostatic interaction with the CD site is absent (Chang et al., 2002; Garai et al., 2012). This demonstrates a critical point in MAPK selectivity: the mechanism of KIM binding to p38 is different for each class of regulators (i.e. MAPKKs versus KIM-PTPs).

Based on NMR and SAXS data, the interaction of resting-state p38 with PTPSL is similar to that described previously between p38 and HePTP. However, the p38 :PTPSL and p38 :HePTP interactions are not identical. One key feature of the p38 :HePTP interaction, the extensive interaction between p38 and the HePTP_{KIS}, is not observed between p38 and the PTPSL_{KIS} (Francis et al., 2011a). Despite the limited interaction surface between p38 and PTPSL, PTPSL binds p38 nearly 6-times tighter than HePTP. Recently published *in vitro* phosphatase assays showed that while HePTP and PTPSL can both readily dephosphorylate p38 , PTPSL is the most efficient p38 phosphatase of all tested (Zhang et al., 2011). This is likely the product of: 1) the highest affinity interaction with p38 among the KIM-PTPs and 2) the limited interaction outside of the KIM, imposing minimal constraints on the flexibility and movement of the PTPSL_{CAT}.

In contrast, the p38 :STEP resting-state complex is more compact than the other two p38 :KIM-PTP resting-state complexes due to an additional previously unidentified interaction between STEP_{CAT} and p38 . In the resting-state complex, STEP_{CAT} occludes a pocket on p38 formed between the MAPK-insert and the C-lobe that has been shown to bind allosteric signaling molecules that are known activators of the p38 cascade, such as fatty acids (Diskin et al., 2008; Nony et al., 2005; Perry et al., 2009). Binding of certain lipid-based molecules to this pocket have been shown to promote auto-phosphorylation and activation of p38 *in vitro* (Gills et al., 2007; Tzarum et al., 2012). STEP regulates p38 at the site of extra-synaptic glutamate receptors, where over-activation of the kinase leads to the production of pro-apoptotic signals culminating in neuronal cell death (Poddar et al., 2010). Therefore, STEP may have adapted several means to suppress p38 activity in the resting-state. First, by binding strongly to the KIM-binding site, STEP prevents upstream activating kinases from promiscuously binding and activating p38 . Second, by blocking access to the MAPK-insert pocket, through the STEP_{CAT} interaction, STEP can prevent the binding of allosteric signaling molecules that induce auto-activation of p38 .

The orientation of STEP_{CAT} in the p38 :STEP resting-state complex is not conducive to dephosphorylation of the tyrosine residue in the p38 phosphorylation loop and significant rotation of STEP_{CAT} is necessary to properly position the active site for catalysis. This domain rearrangement is evident when comparing SAXS data of the resting- and active-states of the p38 :STEP complex. A study conducted by Zhang et al. showed that STEP is significantly less efficient than PTPSL and HePTP at dephosphorylating p38 . The k_{cat} for the STEP-catalyzed dephosphorylation of p38 is ~20-fold lower than those for PTPSL or HePTP, showing that it is likely easier to move the flexibly-tethered HePTP_{CAT} and PTPSL_{CAT} than moving the “trapped” (i.e. p38 bound) STEP_{CAT} (Balasu et al., 2009; Zhang et al., 2011).

Taken together, these results provide fundamental new insights into the molecular basis of p38 regulation by the neuronal KIM-PTPs. We have identified a novel means by which STEP prevents promiscuous activation of p38 by blocking access to the MAPK-insert pocket. As p38 has been implicated in the pathogenesis of numerous neurological disorders, these findings could facilitate the development of new drug therapies to treat these disorders.

EXPERIMENTAL PROCEDURES

Peptide and protein preparation

The PTPSL_{KIM} peptide (IGLQERRGSNVSLTLDM), STEP_{KIM} (MGLQERRGSNVSLTLDM) and STEP_{KIMKIS} (MGLQERRGSNVSLTLDMCTPGCNEEGFGYLVSPREESAHEYLLS) were synthesized, HPLC purified and verified by mass spectrometry (MS) (>98% purity; Biosynthesis, Inc.).

Expression and purification of unphosphorylated p38 was carried out as previously described (Francis et al., 2011a). PTPSL (residues 332–655), PTPSL_{CAT} (residues 361–655), STEP (residues 214–539), STEP_{CAT} (residues 244–539), and PSChimera (PTPSL residues 332–373 with STEP residues 257–539; gene synthesized by DNA 2.0) were expressed and purified using the protocol previously described in detail for STEP_{CAT} (Francis et al., 2013). STEP (residues 214–539) mutants F274A/F281A, F280A/I307A and M285A/I307A were produced by quick-change mutagenesis.

The PTPSL_{KIMKIS} (residues 332–373) was subcloned into a derivative of the pET28 vector that includes an N-terminal His₆-tag and a TEV protease recognition sequence (Peti and Page, 2007). The expression vector was transformed into BL21-(DE3) RIL *E. coli* cells

(Invitrogen). Cultures were grown in Luria broth at 37°C with shaking at 250 rpm until reaching an optical density (OD₆₀₀) between 0.6–0.8, at which point expression was induced by the addition of 1.0 mM isopropylthio- β -D-galactoside (IPTG, final concentration). The cultures were grown for an additional 3 hours at 37 °C with shaking at 250 rpm. The cells were harvested by centrifugation (6000 $\times g$, 12 min, 4°C) and stored at –80°C until purification. All buffers and glassware used for purification were autoclaved prior to purification. For purification, cell pellets were resuspended in lysis buffer (50 mM Tris pH 8.0, 500 mM NaCl, 5 mM imidazole, 0.1% Triton X-1000, and cOmplete EDTA-free protease inhibitor cocktail tablets; Roche) and lysed by high pressure homogenization (Avestin C3 Emulsiflex). The bacterial lysate was cleared by centrifugation (35000 $\times g$, 40 min, 4°C). After filtration, the supernatant was loaded onto a 5 mL HisTrap HP column (GE Healthcare) equilibrated with Buffer A (50 mM Tris pH 8.0, 500 mM NaCl, 5 mM imidazole). Protein was eluted from the column using a 5–500 mM imidazole gradient over 20 column volumes. Purified fractions were pooled, and the his₆-tag was removed by incubation with TEV protease during overnight dialysis in 50 mM Tris pH 8.0, 500 mM NaCl at 4°C. The TEV protease, the His₆-tag and uncleaved protein were removed using a second IMAC step. Final purification was achieved using size exclusion chromatography (SEC) equilibrated in 50 mM Tris pH 6.8, 500 mM NaCl. The molecular weight of the purified peptide was verified by electrospray-ionization MS.

All unlabeled, purified proteins were stored at –80°C until use at which point they were thawed and equilibrated in the appropriate buffer using SEC. All labeled proteins for NMR analysis were purified within 24 hours of data acquisition and stored on ice. PTPSL_{KIM}, STEP_{KIM} and STEP_{KIMKIS} peptides were solubilized in the appropriate buffer prior to the experiment. The final protein buffer was dependent on the experiment performed. For ITC experiments, the final SEC purification was performed in ITC buffer (10 mM Tris pH 7.5, 150 mM NaCl, 0.1 mM EDTA, 0.5 mM TCEP); for NMR and SAXS experiments, the final SEC purification was performed in NMR buffer (50 mM HEPES pH 6.8, 150 mM NaCl, 5 mM dithiothreitol).

NMR sample preparation

[²H,¹⁵N]-p38 (Vogtherr et al., 2005) and [²H,¹⁵N]-STEP were expressed in M9 media supplemented with ¹⁵NH₄Cl (1 g/l) in 99% D₂O and purified as previously described. PTPSL_{KIM}, PTPSL_{KIMKIS}, STEP_{KIM}, or STEP_{KIMKIS} peptides were added to [²H,¹⁵N]-p38 (100 μ M p38) in the following molar excesses: PTPSL_{KIM} (1:1 and 1:8 molar ratio, p38:peptide), PTPSL_{KIMKIS} (1:1 and 1:3 molar ratio, p38:peptide), STEP_{KIM} (1:1, 1:3, 1:5 and 1:8 molar ratio, p38:peptide) and STEP_{KIMKIS} (1:1, 1:3, 1:6 and 1:8 molar ratio, p38:peptide). PTPSL_{CAT} and STEP_{CAT} were added to [²H,¹⁵N]-p38 (100 μ M p38) in a 2-fold molar excess (0.1 mM [²H,¹⁵N]-p38 :0.2 mM PTPSL_{CAT} or STEP_{CAT}). For p38 :KIM-PTP complex formation, [²H,¹⁵N]-p38 was incubated with either PTPSL, STEP or PSChimera (1:1 molar ratio) on ice for 45 min and purified using SEC (Superdex 75 26/60, NMR buffer). Each p38 :KIM-PTP complex elutes at the position expected for the p38 :KIM-PTP heterodimer. Each [²H,¹⁵N]-p38 :KIM-PTP complex was concentrated to 0.1 mM and stored on ice (<8 hours) until NMR data acquisition. For the p38 :[²H,¹⁵N]-STEP complex formation, [²H,¹⁵N]-STEP was incubated with p38 (1:1 molar ratio) on ice for 45 min and purified using SEC (Superdex 75 26/60, NMR buffer). The p38 :[²H,¹⁵N]-STEP complex was concentrated to 0.1 mM and stored on ice (<2 hours) until NMR data acquisition. A 2D [¹H,¹⁵N]-TROSY spectrum was recorded for all samples described above. All NMR experiments were performed at 298 K on a Bruker Advance 800 MHz spectrometer equipped with a TCI HCN z-gradient cryoprobe. NMR samples were prepared in NMR buffer in 90% H₂O/10% D₂O. The NMR spectra were processed with Topspin 2.1/3.0/3.1 (Bruker, Billerica, MA) and analyzed using CARA (<http://cara.nmr.ch>).

Chemical shift perturbation studies

The p38 :STEP_{KIM} and p38 :PTPSL_{KIM} peptide titration series (1:1, 1:3, 1:5 and 1:8 ratio p38 :STEP_{KIM}) were used to follow chemical shift changes in p38 upon peptide or protein binding. Nearly all peaks showed fast exchange and thus could be easily tracked. The observed trajectory of each peak was applied to the analysis of the KIMKIS peptides (PTPSL_{KIMKIS} and STEP_{KIMKIS}) and the full-length complexes (PTPSL, STEP, and PSChimera) allowing for high certainty of peak assignments of p38 in the bound conformations. All chemical shift differences ($\Delta\delta$) were calculated using

$$\Delta\delta(ppm) = \sqrt{(\Delta\delta_H)^2 + \left(\frac{\Delta\delta_N}{10}\right)^2}$$

To allow for direct comparison across all CSP experiments, we used identical cut-off CSPs as in the HePTP NMR experiments; small CSP 0.07–0.103 ppm, medium CSP 0.104–0.131 ppm; large CSP > 0.132 (Francis et al., 2011a).

HADDOCK Calculations

HADDOCK was used to dock p38 and STEP using ambiguous NMR-derived restraints. p38 (PBDID 1P38) and STEP (PBDID 2BIJ) were used as starting input. Active residues were defined as those that undergo a CSP and have high solvent accessibility in the unbound protein structure (p38 residues: 177, 179, 183, 222, 248, 254, 256; STEP residues: 263, 268, 269, 274, 277, 278, 279, 281, 282, 285, 286, 294, 306, 307, 377, 378, 379, 516, 517, 518). Passive residues are those have a CSP but have low solvent accessibility (p38 residues: 190, 195, 247, 255, 328; STEP residues: 276, 280, 350, 353, 376, 380, 478, 479, 482, 520, 525). CSPs were the only experimental restraint type used in the HADDOCK calculation and default settings were used for all docking steps, as used by the easy interface of the HADDOCK webserver.

Small angle X-ray scattering

For the resting-state p38 :PTPSL and p38 :STEP complexes, purified, unphosphorylated p38 was incubated in a 1:1 molar ratio with purified PTPSL_{331–655} and/or purified STEP_{214–539} on ice for 30 min and the complexes purified using SEC (Superdex 75 26/60, NMR buffer). To form the active-state complex of p38 :STEP, purified, dually-phosphorylated p38 was incubated in a 1:1 molar ratio with purified STEP_{214–539} T306D/C472S on ice for 30 min and the complex was purified using SEC (Superdex 75 26/60, NMR buffer). For p38 :PTPSL, data was collected on samples at 0.4, 0.8, 1.6, 2.3 and 4.0 mg/ml. For resting-state p38 :STEP, data was collected on samples at 1.0, 2.0 and 4.0 mg/ml. For active-state p38 :STEP, data was collected on samples at 0.8, 3.3 and 6.1 mg/ml. All samples were prepared within 48 hours of data acquisition and stored on ice at 4°C. All samples were filtered (0.02 μ m filter, Whatman) immediately prior to data collection. 20 μ l of sample was continuously flowed through a 1 mm diameter capillary and exposed to an X-ray beam for 30 s (p38 :PTPSL), 60 s (active-state p38 :STEP), or 180 s (resting-state p38 :STEP). Normalization for beam intensity, buffer subtraction and merging of the data from both detectors were carried out using PRIMUS (Konarev et al., 2003). A Guinier approximation, $I(q) = I(0)\exp(-q^2R_g^2/3)$, where a plot of $\ln[I(q)]$ and q^2 is linear for $q < 1.3/R_g$, was performed on at least four independent scattering trials and averaged to determine the radius of gyration. The linearity of the Guinier region and the intensity at zero scattering angle, $I(0)$, were used to validate that all samples were monodisperse in solution. $I(0)/c$, where c is concentration, was consistent for all measurements for a single complex. GNOM

(Svergun, 1992) was used to determine the pair-distribution function, $P(r)$, for each complex. Twenty-four envelopes were generated for each complex using GASBOR (Svergun et al., 2001) and were aligned and averaged using the DAMAVER program suite (Volkov and Svergun, 2003).

Supplementary Material

Refer to Web version on PubMed Central for supplementary material.

Acknowledgments

The authors thank Drs. L. Yang and M. Allaire (National Synchrotron Light Source, NSLS) for their support at NSLS beamline X9. We thank Dr. Paul Lombroso, Yale University, for providing PTPN5 DNA. This research was supported by grant RSG-08-067-01-LIB from the American Cancer Society to R.P. and by R01GM100910 from the National Institute of Health to W.P. Use of NSLS at Brookhaven National Laboratory was supported by the US Department of Energy, Office of Science, Office of Basic Energy Sciences under contract no. DE-AC02-98CH10886. 800 MHz NMR data were recorded at Brandeis University; the instrument was purchased with support from NIH S10-RR017269.

References

- Akella R, Min X, Wu Q, Gardner KH, Goldsmith EJ. The third conformation of p38alpha MAP kinase observed in phosphorylated p38alpha and in solution. *Structure*. 2010; 18:1571–1578. [PubMed: 21134636]
- Balasu MC, Spiridon LN, Miron S, Craescu CT, Scheidig AJ, Petrescu AJ, Szedlacsek SE. Interface analysis of the complex between ERK2 and PTP-SL. *PLoS One*. 2009; 4:e5432. [PubMed: 19424502]
- Blanco-Aparicio C, Torres J, Pulido R. A novel regulatory mechanism of MAP kinases activation and nuclear translocation mediated by PKA and the PTP-SL tyrosine phosphatase. *J Cell Biol*. 1999; 147:1129–1136. [PubMed: 10601328]
- Chang CI, Xu BE, Akella R, Cobb MH, Goldsmith EJ. Crystal structures of MAP kinase p38 complexed to the docking sites on its nuclear substrate MEF2A and activator MKK3b. *Mol Cell*. 2002; 9:1241–1249. [PubMed: 12086621]
- Chirivi RG, Dilaver G, van de Vorstenbosch R, Wanschers B, Schepens J, Croes H, Fransen J, Hendriks W. Characterization of multiple transcripts and isoforms derived from the mouse protein tyrosine phosphatase gene Ptprr. *Genes Cells*. 2004; 9:919–933. [PubMed: 15461663]
- de Vries SJ, van Dijk AD, Krzeminski M, van Dijk M, Thureau A, Hsu V, Wassenaar T, Bonvin AM. HADDOCK versus HADDOCK: new features and performance of HADDOCK2.0 on the CAPRI targets. *Proteins*. 2007; 69:726–733. [PubMed: 17803234]
- Derijard B, Raingeaud J, Barrett T, Wu IH, Han J, Ulevitch RJ, Davis RJ. Independent human MAP-kinase signal transduction pathways defined by MEK and MKK isoforms. *Science*. 1995; 267:682–685. [PubMed: 7839144]
- Diskin R, Engelberg D, Livnah O. A novel lipid binding site formed by the MAP kinase insert in p38 alpha. *J Mol Biol*. 2008; 375:70–79. [PubMed: 17999933]
- Dominguez C, Boelens R, Bonvin AM. HADDOCK: a protein-protein docking approach based on biochemical or biophysical information. *J Am Chem Soc*. 2003; 125:1731–1737. [PubMed: 12580598]
- Eswaran J, von Kries JP, Marsden B, Longman E, Debreczeni JE, Ugochukwu E, Turnbull A, Lee WH, Knapp S, Barr AJ. Crystal structures and inhibitor identification for PTPN5, PTPRR and PTPN7: a family of human MAPK-specific protein tyrosine phosphatases. *Biochem J*. 2006; 395:483–491. [PubMed: 16441242]
- Francis DM, Page R, Peti W. Sequence-specific backbone 1H, 13C and 15N assignments of the 34 kDa catalytic domain of PTPN5 (STEP). *Biomol NMR Assign*. 2013 Submitted.

- Francis DM, Rozycki B, Koveal D, Hummer G, Page R, Peti W. Structural basis of p38alpha regulation by hematopoietic tyrosine phosphatase. *Nat Chem Biol.* 2011a; 7:916–924. [PubMed: 22057126]
- Francis DM, Rozycki B, Tortajada A, Hummer G, Peti W, Page R. Resting and active states of the ERK2:HePTP complex. *J Am Chem Soc.* 2011b; 133:17138–17141. [PubMed: 21985012]
- Garai A, Zeke A, Gogl G, Toro I, Fordos F, Blankenburg H, Barkai T, Varga J, Alexa A, Emig D, et al. Specificity of linear motifs that bind to a common mitogen-activated protein kinase docking groove. *Sci Signal.* 2012; 5:ra74. [PubMed: 23047924]
- Gills JJ, Castillo SS, Zhang C, Petukhov PA, Memmott RM, Hollingshead M, Warfel N, Han J, Kozikowski AP, Dennis PA. Phosphatidylinositol ether lipid analogues that inhibit AKT also independently activate the stress kinase, p38alpha, through MKK3/6-independent and -dependent mechanisms. *J Biol Chem.* 2007; 282:27020–27029. [PubMed: 17631503]
- Hendriks W, Schepens J, Brugman C, Zeeuwen P, Wieringa B. A novel receptor-type protein tyrosine phosphatase with a single catalytic domain is specifically expressed in mouse brain. *Biochem J.* 1995; 305(Pt 2):499–504. [PubMed: 7832766]
- Kim EK, Choi EJ. Pathological roles of MAPK signaling pathways in human diseases. *Biochim Biophys Acta.* 2010; 1802:396–405. [PubMed: 20079433]
- Konarev PV, Volkov VV, Sokolova AV, Koch MHJ, Svergun DI. PRIMUS: a Windows PC-based system for small-angle scattering data analysis. *Journal of Applied Crystallography.* 2003; 36:1277–1282.
- Kozin MB, Svergun DI. Automated matching of high- and low-resolution structural models. *Journal of Applied Crystallography.* 2001; 34:33–41.
- Larkin MA, Blackshields G, Brown NP, Chenna R, McGettigan PA, McWilliam H, Valentin F, Wallace IM, Wilm A, Lopez R, et al. Clustal W and Clustal X version 2.0. *Bioinformatics.* 2007; 23:2947–2948. [PubMed: 17846036]
- Lombroso PJ, Murdoch G, Lerner M. Molecular characterization of a protein-tyrosine-phosphatase enriched in striatum. *Proc Natl Acad Sci U S A.* 1991; 88:7242–7246. [PubMed: 1714595]
- Lombroso PJ, Naegele JR, Sharma E, Lerner M. A protein tyrosine phosphatase expressed within dopaminergic neurons of the basal ganglia and related structures. *J Neurosci.* 1993; 13:3064–3074. [PubMed: 8331384]
- Munoz JJ, Tarrega C, Blanco-Aparicio C, Pulido R. Differential interaction of the tyrosine phosphatases PTP-SL, STEP and HePTP with the mitogen-activated protein kinases ERK1/2 and p38alpha is determined by a kinase specificity sequence and influenced by reducing agents. *Biochem J.* 2003; 372:193–201. [PubMed: 12583813]
- Mustelin T, Tautz L, Page R. Structure of the hematopoietic tyrosine phosphatase (HePTP) catalytic domain: structure of a KIM phosphatase with phosphate bound at the active site. *J Mol Biol.* 2005; 354:150–163. [PubMed: 16226275]
- Nielsen G, Schwalbe H. NMR spectroscopic investigations of the activated p38 mitogen-activated protein kinase. *ChemBiochem.* 2011; 12:2599–2607. [PubMed: 22012687]
- Nony PA, Kennett SB, Glasgow WC, Olden K, Roberts JD. 15S-Lipoxygenase-2 mediates arachidonic acid-stimulated adhesion of human breast carcinoma cells through the activation of TAK1, MKK6, and p38 MAPK. *J Biol Chem.* 2005; 280:31413–31419. [PubMed: 16000313]
- Ortega A, Amoros D, Garcia de la Torre J. Prediction of hydrodynamic and other solution properties of rigid proteins from atomic- and residue-level models. *Biophys J.* 2011; 101:892–898. [PubMed: 21843480]
- Perry JJ, Harris RM, Moiani D, Olson AJ, Tainer JA. p38alpha MAP kinase C-terminal domain binding pocket characterized by crystallographic and computational analyses. *J Mol Biol.* 2009; 391:1–11. [PubMed: 19501598]
- Peti W, Page R. Strategies to maximize heterologous protein expression in *Escherichia coli* with minimal cost. *Protein Expr Purif.* 2007; 51:1–10. [PubMed: 16904906]
- Piserchio A, Francis DM, Koveal D, Dalby KN, Page R, Peti W, Ghose R. Docking Interactions of Hematopoietic Tyrosine Phosphatase with MAP Kinases ERK2 and p38alpha. *Biochemistry.* 2012; 51:8047–8049. [PubMed: 23030599]

- Poddar R, Deb I, Mukherjee S, Paul S. NR2B-NMDA receptor mediated modulation of the tyrosine phosphatase STEP regulates glutamate induced neuronal cell death. *Journal of neurochemistry*. 2010; 115:1350–1362. [PubMed: 21029094]
- Saxena M, Williams S, Tasken K, Mustelin T. Crosstalk between cAMP-dependent kinase and MAP kinase through a protein tyrosine phosphatase. *Nat Cell Biol*. 1999; 1:305–311. [PubMed: 10559944]
- Svergun D. Determination of the regularization parameter in indirect-transform methods using perceptual criteria. *Journal of Applied Crystallography*. 1992; 25:495–503.
- Svergun DI, Petoukhov MV, Koch MH. Determination of domain structure of proteins from X-ray solution scattering. *Biophys J*. 2001; 80:2946–2953. [PubMed: 11371467]
- Szedlacsek SE, Aricescu AR, Fulga TA, Renault L, Scheidig AJ. Crystal structure of PTP-SL/PTPBR7 catalytic domain: implications for MAP kinase regulation. *J Mol Biol*. 2001; 311:557–568. [PubMed: 11493009]
- Tarrega C, Blanco-Aparicio C, Munoz JJ, Pulido R. Two clusters of residues at the docking groove of mitogen-activated protein kinases differentially mediate their functional interaction with the tyrosine phosphatases PTP-SL and STEP. *J Biol Chem*. 2002; 277:2629–2636. [PubMed: 11711538]
- Tzarum N, Eisenberg-Domovich Y, Gills JJ, Dennis PA, Livnah O. Lipid molecules induce p38alpha activation via a novel molecular switch. *J Mol Biol*. 2012; 424:339–353. [PubMed: 23079240]
- Van Den Maagdenberg AM, Bachner D, Schepens JT, Peters W, Franssen JA, Wieringa B, Hendriks WJ. The mouse Ptprr gene encodes two protein tyrosine phosphatases, PTP-SL and PTPBR7, that display distinct patterns of expression during neural development. *The European journal of neuroscience*. 1999; 11:3832–3844. [PubMed: 10583472]
- Vogtherr M, Saxena K, Grimme S, Betz M, Schieberr U, Pescatore B, Langer T, Schwalbe H. NMR backbone assignment of the mitogen-activated protein (MAP) kinase p38. *J Biomol NMR*. 2005; 32:175. [PubMed: 16034669]
- Volkov VV, Svergun DI. Uniqueness of ab initio shape determination in small-angle scattering. *Journal of Applied Crystallography*. 2003; 36:860–864.
- Wang Z, Harkins PC, Ulevitch RJ, Han J, Cobb MH, Goldsmith EJ. The structure of mitogen-activated protein kinase p38 at 2.1-A resolution. *Proc Natl Acad Sci U S A*. 1997; 94:2327–2332. [PubMed: 9122194]
- Xu J, Kurup P, Zhang Y, Goebel-Goody SM, Wu PH, Hawasli AH, Baum ML, Bibb JA, Lombroso PJ. Extrasynaptic NMDA receptors couple preferentially to excitotoxicity via calpain-mediated cleavage of STEP. *J Neurosci*. 2009; 29:9330–9343. [PubMed: 19625523]
- Zanke B, Suzuki H, Kishihara K, Mizzen L, Minden M, Pawson A, Mak TW. Cloning and expression of an inducible lymphoid-specific, protein tyrosine phosphatase (HePTPase). *Eur J Immunol*. 1992; 22:235–239. [PubMed: 1530918]
- Zhang YY, Wu JW, Wang ZX. Mitogen-activated protein kinase (MAPK) phosphatase 3-mediated cross-talk between MAPKs ERK2 and p38alpha. *J Biol Chem*. 2011; 286:16150–16162. [PubMed: 21454500]
- Zhou T, Sun L, Humphreys J, Goldsmith EJ. Docking interactions induce exposure of activation loop in the MAP kinase ERK2. *Structure*. 2006; 14:1011–1019. [PubMed: 16765894]

Highlights

- The p38 :PTPSL interaction is confined mainly to the KIM-binding site.
- The p38 :PTPSL complex adopts an extended conformation.
- The STEP catalytic domain interacts with a novel p38 binding site.
- The p38 :STEP resting- and active-states have distinct conformations.

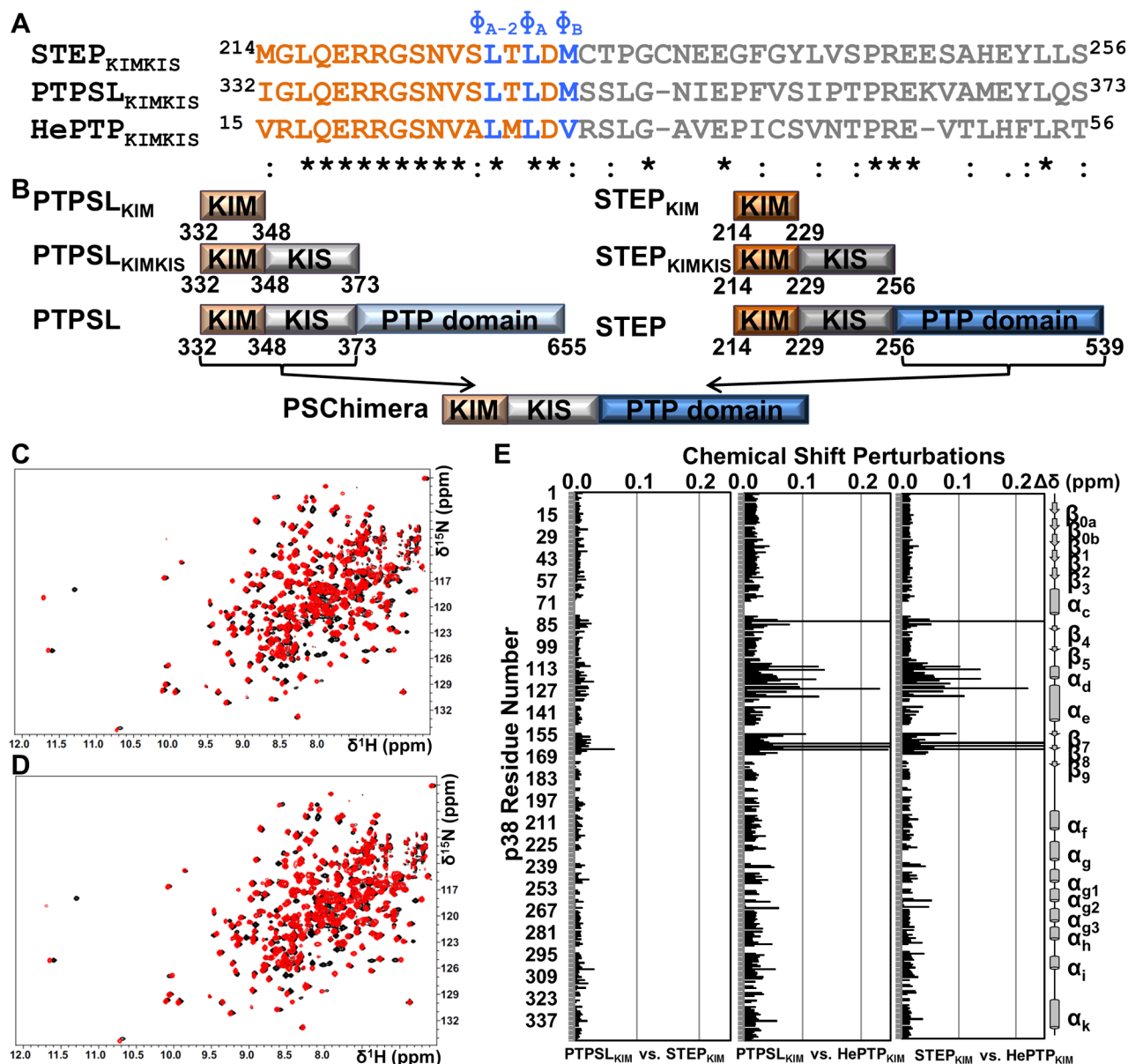


Figure 1. The mode of KIM binding is conserved within the KIM-PTP family
 (A) Sequences of STEP_{KIMKIS}, PTPSL_{KIMKIS}, and HePTP_{KIMKIS} and conservation as determined using ClustalW (Larkin et al., 2007). KIM residues are colored in orange and blue. KIS residues are colored in gray. (B) Constructs used in this study. (C) 2D [¹H,¹⁵N] TROSY spectrum of [²H,¹⁵N]-p38 (black) overlaid with the 2D [¹H,¹⁵N] TROSY spectrum of [²H,¹⁵N]-p38 :PTPSL_{KIM} (red; 1:8 molar ratio p38 :PTPSL_{KIM}) (D) 2D [¹H,¹⁵N] TROSY spectrum of [²H,¹⁵N]-p38 (black) overlaid with the 2D [¹H,¹⁵N] TROSY spectrum of [²H,¹⁵N]-p38 :STEP_{KIM} (red; 1:8 molar ratio p38 :STEP_{KIM}) (E) Histograms which show the combined ¹H/¹⁵N CSPs vs. p38 residue for the final titration points of each KIM-PTP_{KIM} peptide with [²H,¹⁵N]-p38. See also Figure S1.

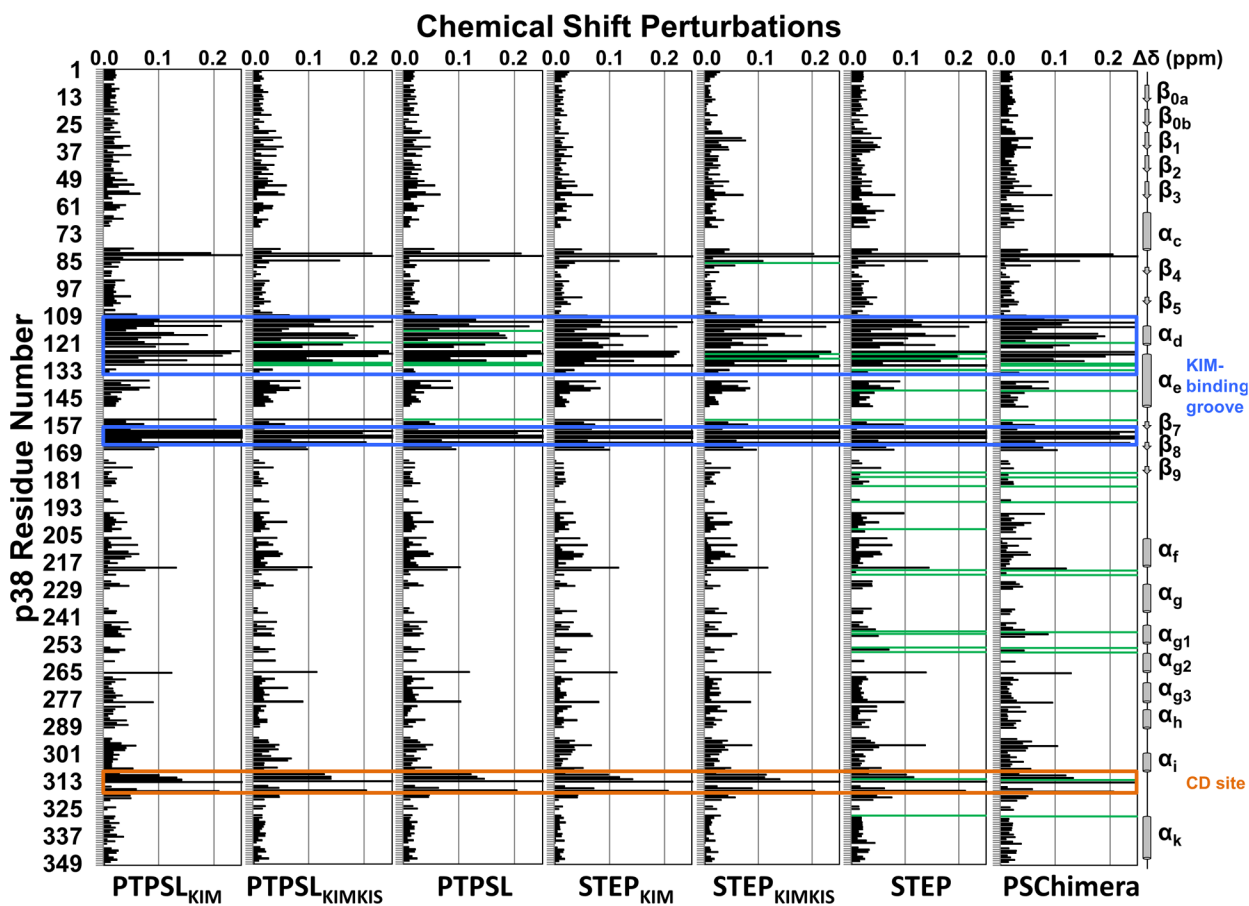


Figure 2. PTPSL and STEP interaction with p38

Histograms showing the combined $^1\text{H}/^{15}\text{N}$ CSP vs. p38 residue for the following experiments: p38 with PTPSL_{KIM} (1:8 molar ratio), PTPSL_{KIMKIS} (1:3 molar ratio), PTPSL (1:1 ratio; SEC purified), STEP_{KIM} (1:8 molar ratio), STEP_{KIMKIS} (1:8 molar ratio), STEP (1:1 ratio; SEC purified), and PSChimera (1:1 ratio; SEC purified). Residues that form the p38 hydrophobic docking groove and the CD site are highlighted by blue and orange boxes, respectively. Residues with peak line-widths broadened beyond detection upon titration are colored in green. See also Figure S2.

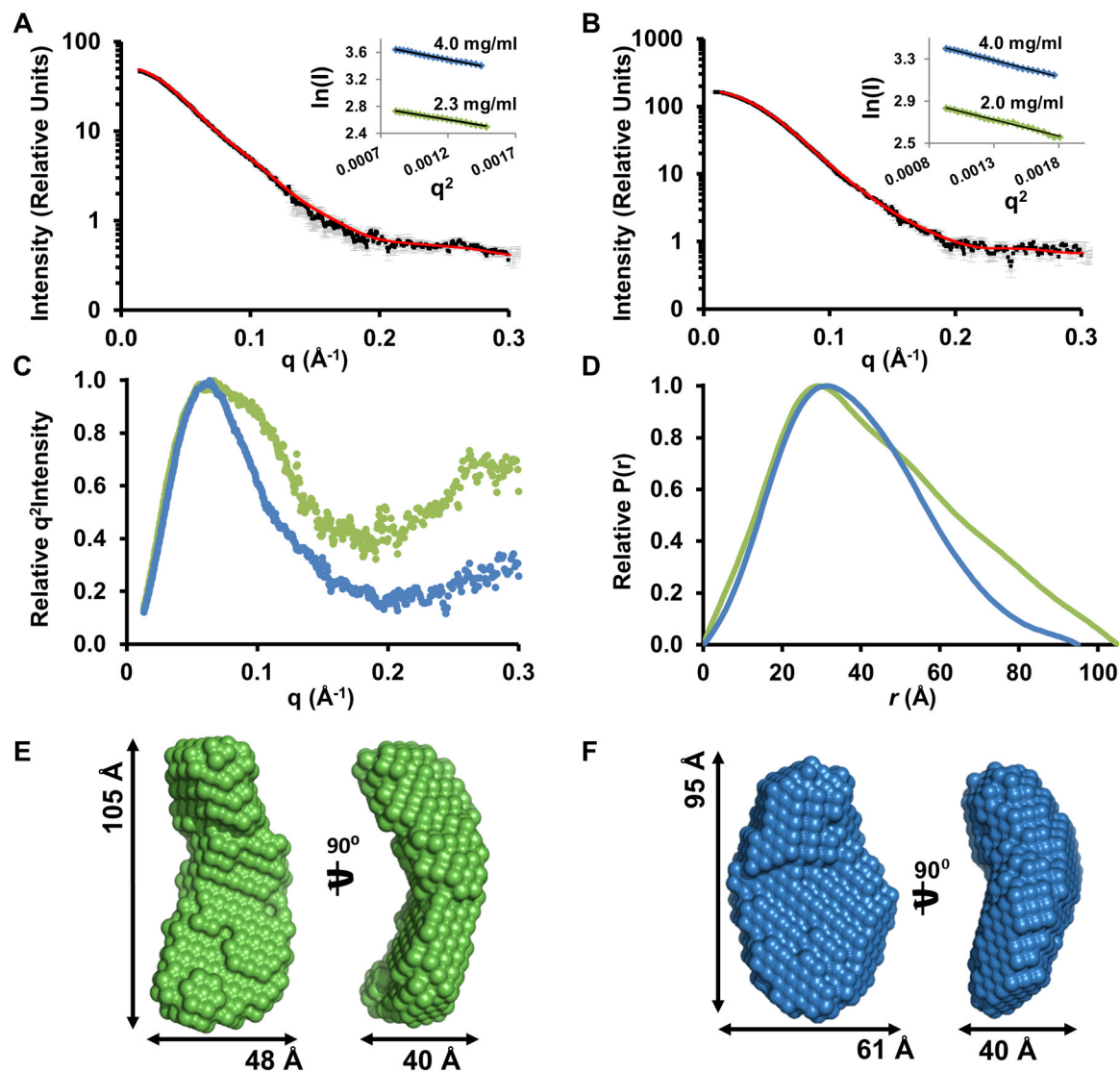


Figure 3. The p38:PTPSL and p38:STEP resting-state complex

(A) SAXS data ($I(q)$ vs q) of the p38:PTPSL resting-state complex shown (black squares) with error bars (grey lines). Error bars show the experimental error based on circular averaging of the 2D solution scattering data; theoretical scattering curve from *ab initio* molecular envelope (red); *inset*, Guinier plots for samples at 2.3 mg/ml and 4.0 mg/ml. (B) SAXS data ($I(q)$ vs q) of the p38:STEP resting-state complex shown (black squares) with error bars (grey lines). Theoretical scattering curve from the *ab initio* molecular envelope (red); *inset*, Guinier plots for samples at 2.0 mg/ml and 4.0 mg/ml. (C) Kratky plot of the p38:PTPSL resting-state SAXS data (green) and p38:STEP resting-state SAXS data (blue). (D) $P(r)$ function of the p38:PTPSL resting-state complex (green) and p38:STEP resting-state complex (blue). (E) p38:PTPSL *ab initio* molecular envelope in two views rotated by 90° with the dimensions of the envelope. (F) The p38:STEP *ab initio* molecular envelope in two views rotated by 90° with the dimensions of the envelope.

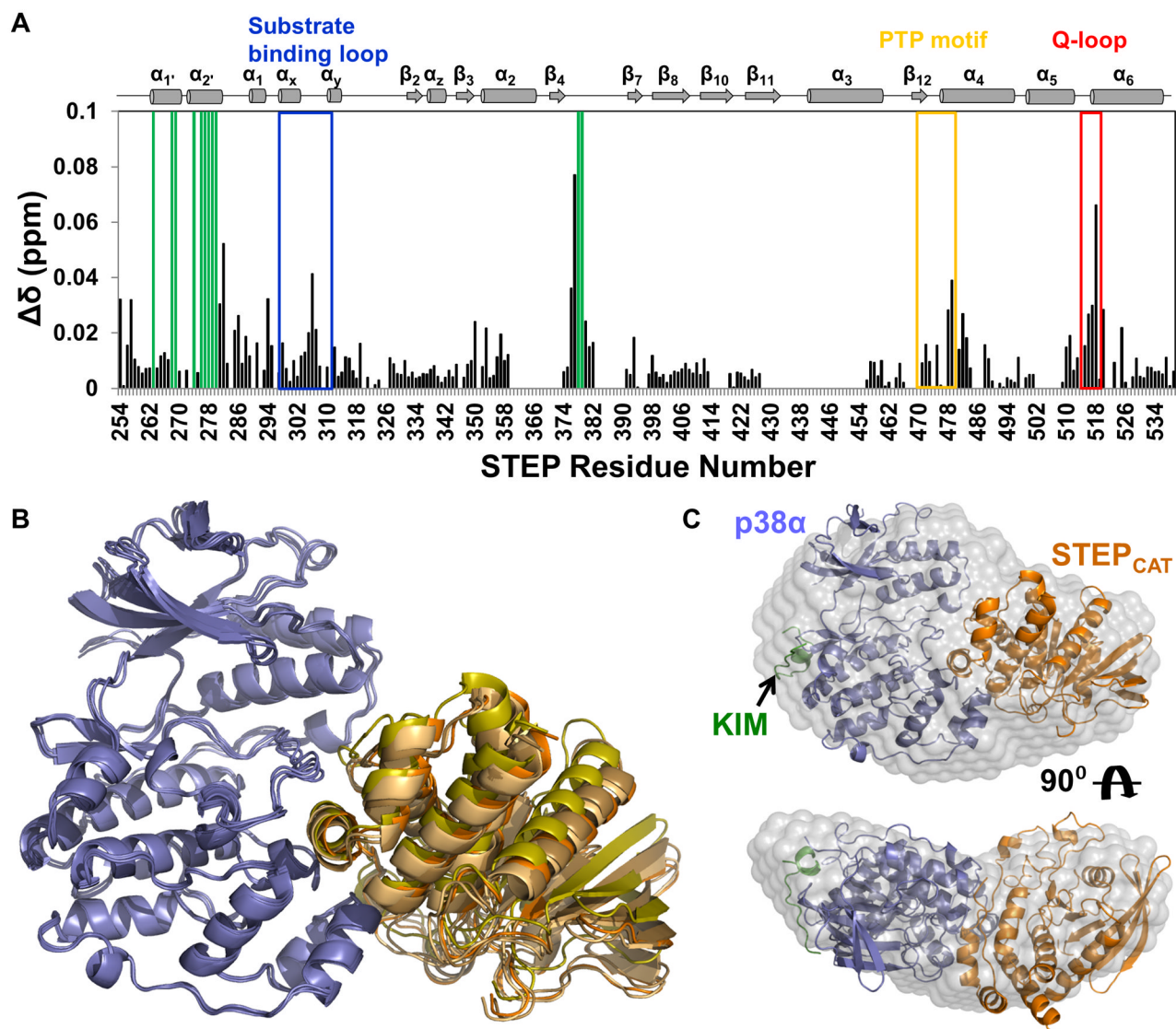


Figure 4. STEP_{CAT} binds to the p38 α activation loop and MAPK-insert primarily through helix -2

(A) Histograms showing the combined $^1\text{H}/^{15}\text{N}$ CSP vs. STEP residue for the interaction of p38 α with $[\text{2H}, \text{15N}]$ -STEP. (B) Alignment of the 4 lowest energy HADDOCK structures of the p38 α :STEP_{CAT} complex. p38 α is colored blue and STEP_{CAT} is colored in shades of orange. (C) Superposition of the lowest energy HADDOCK p38 α :STEP_{CAT} complex structure with the experimental SAXS molecular envelope of the p38 α :STEP resting-state complex; p38 α (blue), KIM (green) and STEP_{CAT} (orange). See also Figure S4.

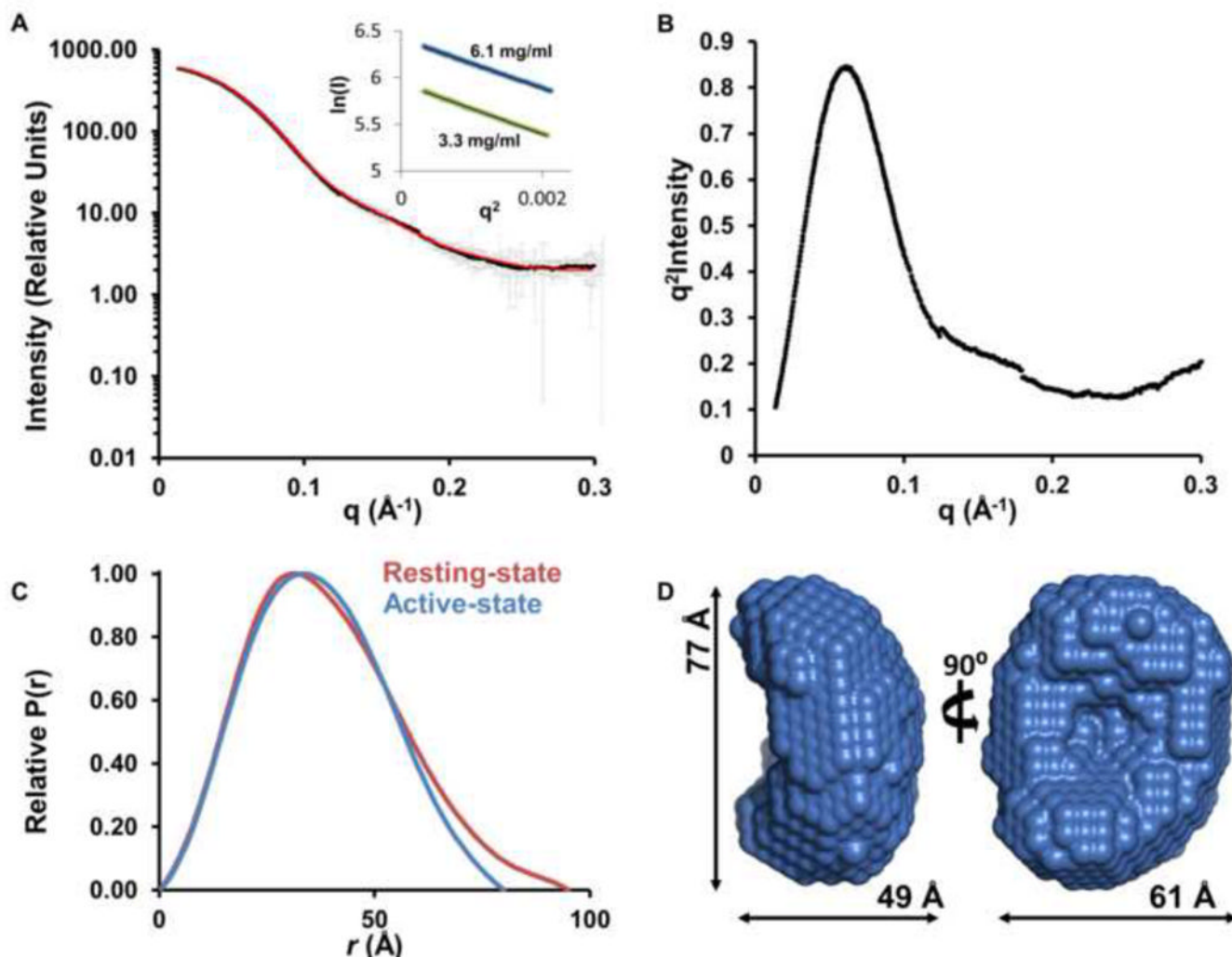


Figure 5. The p38 :STEP active-state complex is more compact than the resting-state complex
 (A) Experimental SAXS data ($I(q)$ vs q) of the p38 :STEP active-state complex shown as black squares with error bars as grey lines; theoretical scattering curve from *ab initio* molecular envelope (red); *inset*, Guinier plots for samples at 3.3 mg/ml and 6.1 mg/ml. (B) Kratky plot. (C) $P(r)$ function of the p38 :STEP active-state complex (blue) overlaid with resting-state complex (red). (D) Averaged *ab initio* molecular envelope; 2 views rotated by 90° with the dimensions of the envelope.

Table 1

Thermodynamic and dissociation constants for p38 :KIM-PTP domains derived from ITC experiments at 25 °C. See also Figure S2.

Interaction	K_d (nM)	H (kcal·mol⁻¹)	T S (kcal·mol⁻¹)	G (kcal·mol⁻¹)
p38 : STEP _{KIM}	3567 ± 208	-37.7 ± 2.5	-30.2 ± 2.5	-7.4 ± 0.1
p38 : STEP _{KIMKIS}	1340 ± 135	-34.7 ± 1.4	-26.6 ± 1.5	-8.0 ± 0.1
p38 : STEP	577 ± 71	-28.8 ± 2.0	-20.3 ± 2.0	-8.5 ± 0.1
p38 : STEP _{F274A/F281A}	1074 ± 105	-24.2 ± 0.4	-16.0 ± 0.4	-8.2 ± 0.1
p38 : STEP _{F281A/I307A}	1062 ± 36	-34.3 ± 1.1	-26.2 ± 1.0	-8.2 ± 0.1
p38 : STEP _{M285A/I307A}	592 ± 106	-27.6 ± 0.5	-19 ± 0.3	-8.5 ± 0.1
p38 : PTPSL _{KIM}	2840 ± 135	-33.0 ± 1.7	-25.4 ± 1.7	-7.6 ± 0.1
p38 : PTPSL _{KIMKIS}	1527 ± 23	-38.8 ± 6.1	-30.8 ± 6.1	-7.9 ± 0.1
p38 : PTPSL	382 ± 65	-30.2 ± 1.5	-21.4 ± 1.4	-8.8 ± 0.1
p38 : PSChimera	309 ± 4	-27.2 ± 0.7	-18.3 ± 0.7	-8.9 ± 0.0

Table 2

SAXS analysis of p38 :PTPRR, p38 :STEP and pp38 :STEP complexes.

	p38:PTPRR	p38:STEP (Resting)	pp38:STEP (Active)
Guinier approximation			
R_g (Å)	33.1 ± 0.5	29.9 ± 0.3	28.5 ± 0.3
P(r) function calculation			
Q-range (Å ⁻¹)	0.013–0.303	0.013–0.304	0.014–0.297
R_g (Å)	34.1	29.8	28.2
D_{max} (Å)	105	95	80
Structure modeling			
	1.4 ± 0.1	1.9 ± 0.2	1.0 ± 0.1
NSD	1.30 ± 0.04	1.09 ± 0.03	1.00 ± 0.03